ISSN 1674-1056
http://cpb.iphy.ac.cn
http://iopscience.iop.org/cpb
中国物理 B
Chinese Physics
中国物理
Chinese Physics B

Ejecta from periodic grooved Sn surface under unsupported shocks

Wen-Bin Liu(刘文斌), Dong-Jun Ma(马东军), An-Min He(何安民), Pei Wang(王裴)
Citation: Chin. Phys. B . 2018, 27(1): 016202. **doi:** 10.1088/1674-1056/27/1/016202

Journal homepage: http://cpb.iphy.ac.cn; http://iopscience.iop.org/cpb

What follows is a list of articles you may be interested in

Influence of shockwave profile on ejecta from shocked Pb surface: Atomistic calculations

Guo-Wu Ren(任国武), Shi-Wen Zhang(张世文), Ren-Kai Hong(洪仁楷), Tie-Gang Tang(汤铁钢), Yong-Tao Chen(陈永涛)
Chin. Phys. B . 2016, 25(8): 086202. **doi:** 10.1088/1674-1056/25/8/086202

Experimental and theoretical analysis of package-on-package structure under three-point bending loading

Jia Su, Wang Xi-Shu, Ren Huai-Hui
Chin. Phys. B . 2012, 21(12): 126201. **doi:** 10.1088/1674-1056/21/12/126201

Ejecta from periodic grooved Sn surface under unsupported shocks*

Wen-Bin Liu(刘文斌)[1,2], Dong-Jun Ma(马东军)[1], An-Min He(何安民)[1], and Pei Wang(王裴)[1,†]

[1] *Institute of Applied Physics and Computational Mathematics, Beijing* 100094, *China*
[2] *Graduate School of China Academy of Engineering Physics, Beijing* 100088, *China*

(Received 18 June 2017; revised manuscript received 25 August 2017; published online 28 November 2017)

Dynamic failure and ejection characteristics of a periodic grooved Sn surface under unsupported shock loading are studied using a smoothed particle hydrodynamics method. An "Eiffel Tower" spatial structure is observed, which is composed of high-speed jet tip, high-density jet slug, longitudinal tensile sparse zone, and complex broken zone between grooves. It is very different from the spike–bubble structure under supported shocks, and has been validated by detonation loading experiments. In comparison with that under supported shocks at the same peak pressure, the high-speed ejecta decreases obviously, whereas the truncated location of ejecta moves towards the interior of the sample and the total mass of ejecta increases due to the vast existence of low-speed broken materials. The shock wave profile determines mainly the total ejection amount, while the variation of V-groove angle will significantly alter the distribution of middle- and high-speed ejecta, and the maximum ejecta velocity has a linear correlation with the groove angle.

Keywords: ejecta, grooved Sn surface, "Eiffel Tower" structure, unsupported shock

PACS: 62.20.M–, 62.50.Ef, 47.20.Ma **DOI:** 10.1088/1674-1056/27/1/016202

1. Introduction

Ejecta can be produced when a shock wave reflects from a metallic surface with imperfections where particulate fragments will be separated from the bulk and ejected outside the free surface at a higher velocity.[1,2] Ejecta formation is thought to be a limiting case of the Richtmyer–Meshkov instability (RMI) at a metal–vacuum (or gas) interface.[3,4] Because of potential damage and mixing impacted by these ejecta, this process has many important practical applications like pyrotechnics or inertial confinement fusion, and has motivated considerable research work worldwide.[1–5]

It is a general consensus that the physical mechanism for ejecta production is microjetting from surface imperfections (e.g., grooves, pits, or scratches) on the free surface of shocked metals.[1–5] The mass and velocity distribution of ejecta are relevant to various factors, such as shock strength and surface roughness. Zenller *et al.*[1,6] investigated the effects of shock breakout pressure, surface roughness, and groove angle on the ejecta production from Sn samples. Rességuirer *et al.*[2,7] studied the influence of various interface perturbation conditions on the laser shock-induced microjetting from the grooved metal surface. Chen *et al.*[8] confirmed experimentally the self-similar expansion evolution of ejecta on melted Sn sample subjected to high pressure loading. Chen *et al.*[9] and Shao *et al.*[10,11] simulated the micro-scale microjetting by molecular dynamics method, explained that the jetting fluid is the main mechanism of microjetting qualitatively, and obtained the change rules of microjetting characteristics in a wide range of pressure. Wang *et al.*[12,13] carried out a series of simulations by a smoothed particle hydrodynamics (SPH) method, and found that the ejection factor reaches its maximum at the half groove angle 45 degrees and reduces with the change of groove angle. They also found that the ejection process can be affected by the micro-structure of surface defect, besides the wavelength and depth of periodic grooves.

The previous focus of experimental and numerical research was the ejection behavior and influence factors under supported shocks, but unsupported shocks (shock waves followed by an unloading rarefaction wave) will be formed in high power laser and detonation loading conditions. When unsupported shocks reflect at the sample surface, the microspall will be formed near the free surface under the interaction of the incident unloading and free surface reflecting rarefaction waves, while the microjetting will be generated from the surface with interface defects owing to the RMI. Therefore, the mechanism of ejecta becomes more complicated due to the coupling between the microspall and microjetting. However, there is a little work about these issues and the mechanism of dynamic failure process is still not clear now.

In this paper, we simulate the ejecta production from typical periodic grooved Sn surface under unsupported shock loading, and investigate the dynamic failure process and ejecta characteristics. Furthermore, we analyze the influence of shock profile and groove angle on the total mass, spatial distribution characteristics of ejecta and the maximum velocity of jetting.

*Project supported by the Joint Fund of the National Natural Science Foundation of China and the China Academy of Engineering Physics (Grant No. U1530261), the National Natural Science Foundation of China (Grant Nos. 11402032 and 11502030), and the Science Challenge Project, China (Grant No. TZ2016001).

†Corresponding author. E-mail: wangpei@iapcm.ac.cn

© 2018 Chinese Physical Society and IOP Publishing Ltd

2. Model and method

The geometric model in this paper is Sn that has periodic grooves on the surface, as shown in Fig. 1. The height of sample is 120 μm, the depth of groove is 40 μm, and the angle is 30°–150°. The unsupported shocks with different profile and peak pressure are generated by impacting Sn sample with a flyer and adjusting the flyer thickness and initial impact velocity. In the simulations, the free boundary condition is imposed on the impact direction and the periodic boundary condition is imposed on the directions which are perpendicular to the impact direction.

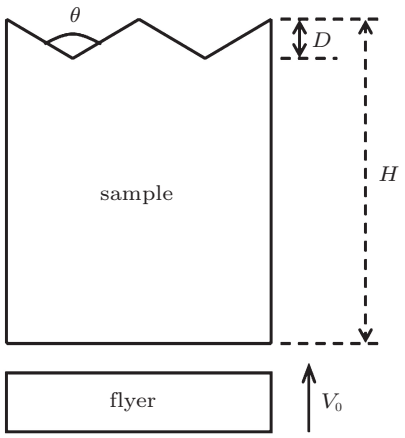


Fig. 1. Calculation model.

Figure 2 is wave profiles about supported shock and unsupported shock at $P_{SB} = 33$ GPa when they reach the bottom of grooves. That the shock wave is supported means that the shock wave is followed by a high pressure platform and the pressure does not decrease with time and distance behind the shock wave. That the shock wave is unsupported means that the shock wave is followed by an unloading rarefaction wave, which looks like a triangular wave, and the pressure decreases with time and distance behind the shock wave. For unsupported shock, the peak value of pressure and unloading velocity are two important parameters. After the flyer of 15 μm thickness impacts the Sn sample at a speed of 2.35 km/s, the shock waves are propagating from the impacting surface to the interior of the flyer and sample respectively after their collision. The unloading rarefaction wave forms and propagates towards the sample when the downwards shock wave arrives at the free bottom surface of the flyer and gradually catches up with the upward traveling shock wave in the sample, which eventually converts to an unsupported shock wave. In the following discussion, the shock pressure is the peak value P_{SB} when the unsupported shock wave reaches the bottom of the grooves.

We simulate the ejecta from the periodic grooved Sn surface using the in-house SPH program developed by Wang *et al.*[12,13] SPH is a Lagrangian particle code which uses no background mesh. In the SPH methodology,[14] smoothed particles are used as interpolation points to represent materials at discrete locations, so it can naturally obtain the history of particles and easily trace material interfaces. For a function f, its function value at a certain location can be expressed as summation interpolants over the neighbor particles using a smoothing kernel function W with the smoothing length h. The meshless nature of SPH methodology overcomes the difficulties due to large deformations. Various applications of SPH have been found in recent years, and it has been extended to high-explosive explosion, hypervelocity impact, and so on.[15,16]

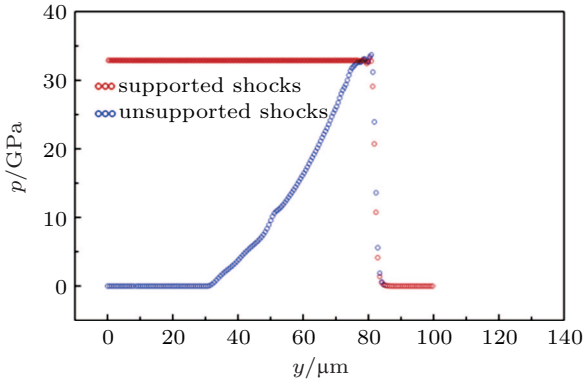


Fig. 2. (color online) Wave profiles about supported shock and unsupported shock at $P_{SB} = 33$ GPa.

The following equations about SPH are used to model the ejecta:

$$\begin{cases} \dfrac{\mathrm{d}\rho_i}{\mathrm{d}t} = \rho_i \sum\limits_j \dfrac{m_j}{\rho_j}\left(U_i^\alpha - U_j^\alpha\right) W_{ij,\alpha}, \\ \dfrac{\mathrm{d}U_i^\alpha}{\mathrm{d}t} = \sum\limits_j m_j \left(\dfrac{\sigma_i^{\alpha\beta}}{\rho_i^2} + \dfrac{\sigma_j^{\alpha\beta}}{\rho_j^2} - \delta^{\alpha\beta} Q_{ij}\right) W_{ij,\beta}, \\ \dfrac{\mathrm{d}e_i}{\mathrm{d}t} = \sum\limits_j m_j \left(U_j^\alpha - U_i^\alpha\right)\left(\dfrac{\sigma_i^{\alpha\beta}}{\rho_i^2} - \dfrac{1}{2}\delta^{\alpha\beta} Q_{ij}\right) W_{ij,\beta}, \end{cases} \tag{1}$$

where $W_{ij,\alpha} = \partial W_{ij}/\partial x_i^\alpha$, $W_{ij,\beta} = \partial W_{ij}/\partial x_i^\beta$, and Q_{ij} is artificial viscosity. The stress tensor can be split up into a hydrostatic pressure part and a deviatoric stress

$$\sigma^{\alpha\beta} = -p\delta^{\alpha\beta} + \tau^{\alpha\beta}. \tag{2}$$

To obtain the deviatoric stress, we calculate the stress rates with the Jaumann stress rate tensor

$$\dot{\tau}^{\alpha\beta} - \tau^{\alpha\gamma} R^{\beta\gamma} - \tau^{\gamma\beta} R^{\alpha\gamma} = 2G\bar{\varepsilon}^{\alpha\beta}, \tag{3}$$

with the strain and rotation rate defined by

$$\varepsilon^{\alpha\beta} = \frac{1}{2}\left(\frac{\partial U^\alpha}{\partial x^\beta} + \frac{\partial U^\beta}{\partial x^\alpha}\right), \tag{4}$$

$$R^{\alpha\beta} = \frac{1}{2}\left(\frac{\partial U^\alpha}{\partial x^\beta} - \frac{\partial U^\beta}{\partial x^\alpha}\right). \tag{5}$$

The hydrostatic pressure part is calculated with metal polynomial equation of state.[14]

For the problem of material fracture, the stress components and pressure are set to zero when the maximum pull stress of the particle reaches the fracture strength and cannot withstand the negative pressure anymore. Metallic polynomial equation of state, Steinberg–Guinan constitutive model, and Lindeman melting law are used in the simulation. The material parameters of Sn are listed in Table 1. The Sn material can be melted with a release shock wave $P_{SB} = 33$ GPa.

Table 1. Material parameters of Sn.

Y_0 /100 GPa	Y_{max} /100 GPa	b /(100 GPa)$^{-1}$	μ_0 /100 GPa	ρ_0 /g·cm^{-3}	h /K^{-1}
1.6×10^{-3}	3×10^{-3}	8.8	0.21	7.3	1.1×10^{-3}
T_{m0}/K	γ_0	β	n		
565	2.36	130	0.1		

3. Ejection characteristic under unsupported shocks

The ejecta at different times in $\theta = 120^\circ$ and $P_{SB} = 33$ GPa are shown in Fig. 3. At 19 ns, the unsupported shock front reaches the bottom of grooves and starts to interact with the grooves. At 24 ns, the bottom of the grooves has been jetting and forms an upward protruding tip, the pressure in jetting area reduces rapidly, and the unsupported shock continues to travel toward the free surface. At 60 ns, the whole grooves have been jetting, the high density jet slug is formed in the middle of ejecta field, and the tensile failure area is generated at the bottom of ejecta field. At 200 ns, it has formed a spatial structure that is similar to "Eiffel Tower", which consists of high-speed jet tip, high-density jet slug, longitudinal tensile sparse zone, and complex broken zone between grooves, marked in Fig. 3. It can be seen clearly that the high-speed jet tip has been broken and the ejecta mass mainly concentrates on the middle jet slug. The longitudinal tensile sparse zone is generated at the bottom of grooves under the interaction between the upward incident and downward free surface release rarefaction waves, while the complex broken zone is generated under the coupling among the incident, the free surface, and the transverse release rarefaction waves between grooves. The similar "Eiffel Tower" spatial structure has been validated by the detonation loading experiments.[17]

The similarities and differences of ejecta are analyzed under supported and unsupported shocks at $\theta = 120^\circ$, $P_{SB} = 33$ GPa, and $t = 200$ ns, as shown in Fig. 4, where the yellow line is the position of theoretical free surface, and the red and green lines are the bottom positions of ejecta statistics under unsupported and supported shocks respectively. It can be seen that the "Eiffel Tower" spatial structure under the unsupported shock is obviously different from the spike–bubble structure under the supported shock. The large regions of longitudinal tensile and broken are formed due to the complex interaction of waves. In contrast with the supported shock case, the truncated location of ejecta moves to the interior of Sn sample due to the coupling of microspall and microjetting.

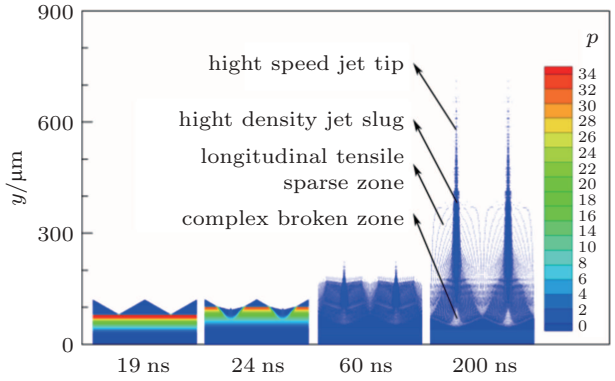


Fig. 3. (color online) Ejecta images in different time under unsupported shock at $P_{SB} = 33$ GPa and $\theta = 120^\circ$.

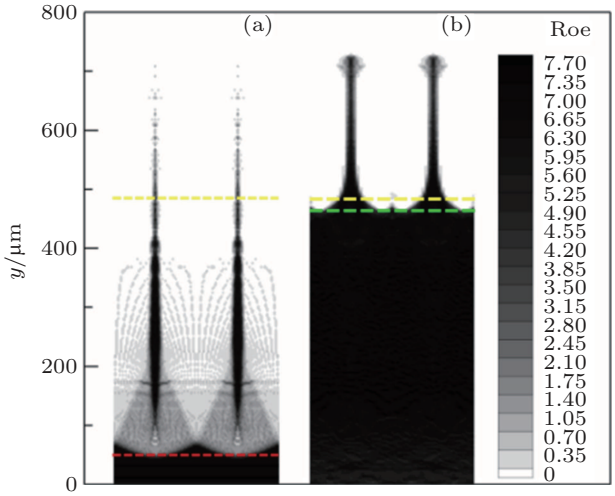


Fig. 4. (color online) Ejecta images under (a) unsupported shock and (b) supported shock at $\theta = 120^\circ$, $P_{SB} = 33$ GPa, and $t = 200$ ns.

The mass and accumulated mass of ejecta along the impacting direction are analyzed under supported and unsupported shocks, as shown in Fig. 5. It can been seen in Fig. 5(a) that the mass of middle-high-speed ejecta under unsupported shock loading is significantly lower than that under supported case because of the decreasing of shock pressure when the release rarefaction wave follows a leading shock wave. There is no distinct boundary between the middle-high-speed ejecta and low-speed broken zone because the main mass of ejection concentrates on the jet slug, whereas there is obvious signal of mass jump between the low-speed broken zone and the dense bulk of Sn sample. The maximum penetration distances of the jet tip for the two shock profiles are almost equal, because the peak pressures are equal when shocks reach the bottom of the grooves. It is shown in Fig. 5(b) that the total mass of ejecta increases under unsupported shock loading because of the existence of large mass of the low-speed zone. For high shock pressure, the Sn releases to a liquid phase and then the dynamic tensile strength of Sn has a significant decrease. Under

unsupported shocks, the interaction of the unloading rarefaction wave behind shock wave with the rarefaction wave reflected from interface leads to a biaxial tension and forms the large mass of the low-speed zone. Under supported shocks, there is not a biaxial tension because of only a rarefaction wave reflected from interface, so the large mass of the speed broken zone is not formed. At the bottom of ejecta statistics, the total mass is 40 mg/cm^2 and the ejection factor is 2.76 under unsupported shock loading, yet the total mass is 20 mg/cm^2 and the ejection factor is 1.38 under supported shock loading.

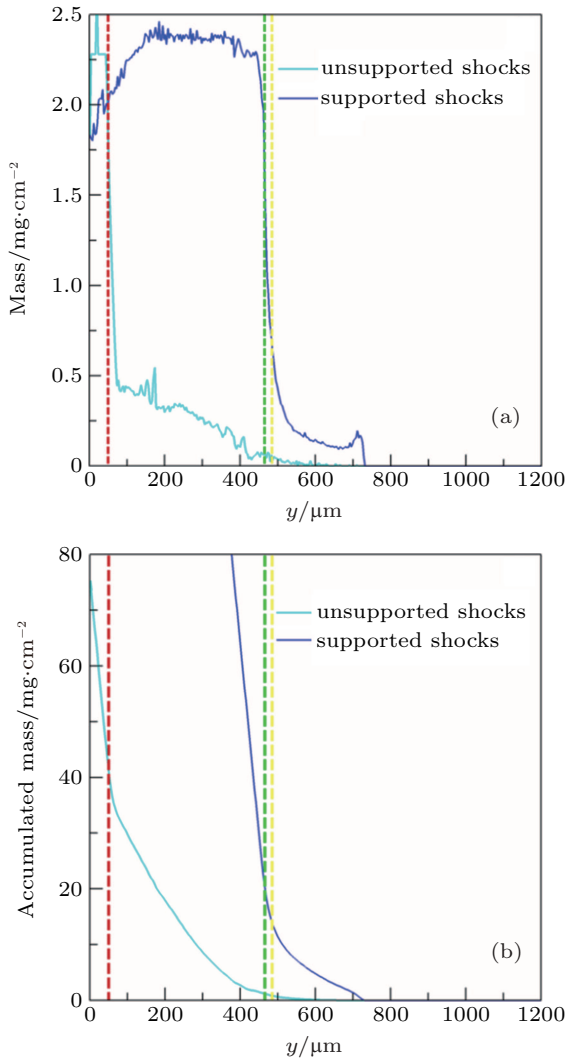


Fig. 5. (color online) Distribution of (a) mass and (b) accumulated mass along impacting direction under unsupported shock and supported shock at $\theta = 120°$, $P_{SB} = 33$ GPa, and $t = 200$ ns.

By tracking the move trail of Lagrangian particles, we analyze the material source of middle-high-speed ejecta. The distributions of material source of ejecta under unsupported and supported shocks are shown in Fig. 6, where the black area is the source region of middle-high-speed ejecta. A lot of ejecta are generated from the whole groove shape under supported shock loading, but only a little jetting product is generated from the bottom of groove under unsupported case because of the decreasing of shock pressure.

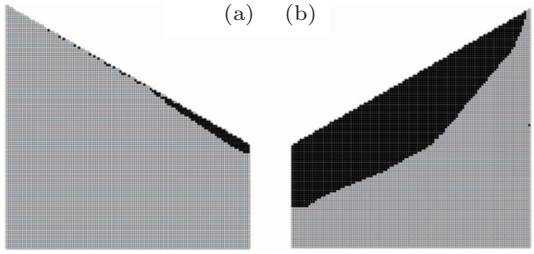


Fig. 6. Material source of ejecta under (a) unsupported shock and (b) supported shock at $\theta = 120°$, $P_{SB} = 33$ GPa, and $t = 200$ ns.

4. Influence of groove angle under unsupported shocks

The simulation results of ejecta with different groove angles at $P_{SB} = 33$ GPa and $t = 410$ ns are shown in Fig. 7. The spatial structures of ejection field with different groove angles are similar, which include high-speed jet tip, high-density jet slug, longitudinal tensile sparse zone, and complex broken zone between grooves. The bottom position of grooves is nearly consistent with varying grooves angles, but the distribution of spatial structure is obviously different. For the high-speed jet tip, the distance and mass of jetting reduce with the increase of groove angle. For the jet slug, there are wing-shaped blocks in small angles (30° and 60°). The incident shock wave has not arrived at the wave crest of the grooves yet and is released by rarefaction wave reflected from the groove edge. Therefore the materials at the wave crest of grooves are not tensile and keep a condensed state, and the materials at the wave trough of grooves get a high velocity and drive the materials on both sides of grooves with a lower velocity. Finally the wing-shaped blocks are formed. With the increase of groove angle, the incident shock wave can arrive at wave crest of grooves, and then the wing-shaped blocks disappear. For the longitudinal tensile sparse zone, the area reaches its minimum at the half angle 45°, and expands with the increase or decrease of groove angle. For the complex broken region between grooves, it does not significantly change with small groove angles (30° and 60°), and the ability of forming complex broken zone is enhanced gradually with the increase of groove angle.

The mass and accumulated mass of ejecta along the impacting direction are also analyzed with different groove angles, shown in Fig. 8, where the black, long dashed line is the position corresponding to the white, long dashed line in Fig. 7. There are dramatic changes in the curve of mass for small groove angle (30° and 60°), because the high-density jet slug exists with wing-shaped blocks. With increasing the angle, the curve becomes smooth. It is shown in Fig. 8(b) that the truncated locations of ejecta statistics are nearly consistent for different groove angles and the total mass is 40 mg/cm^2, which means that the depth of bottom broken region depends on the profile of unsupported shocks. The middle-high-speed

ejecta are obviously influenced by the groove shape and have different growth trends for the accumulated mass with different groove angle.

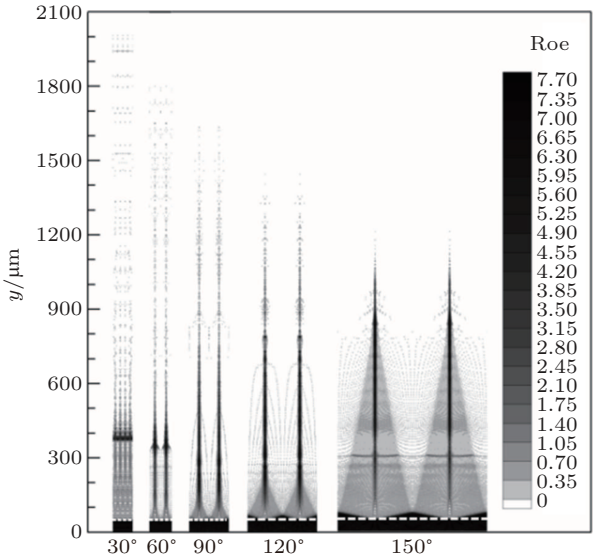


Fig. 7. (color online) Ejecta images with different groove angle at $P_{SB} =$ 33 GPa and $t = 410$ ns.

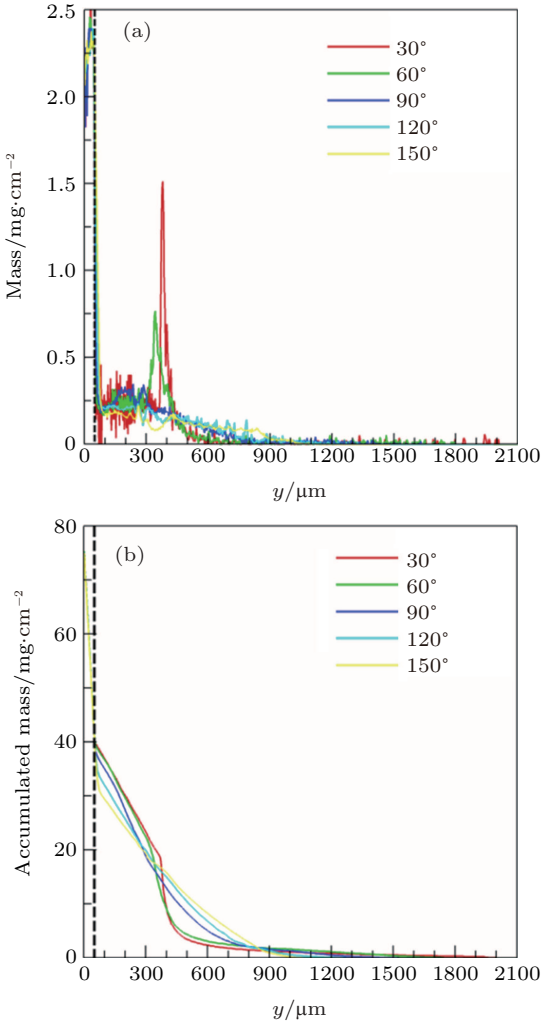


Fig. 8. (color online) Distribution of (a) mass and (b) accumulated mass along impacting direction with different angle under unsupported shock at $P_{SB} = 33$ GPa and $t = 410$ ns.

Finally, the maximum ejecta velocities are extracted in Fig. 9 and show a linear reduction with the increase of groove angle.

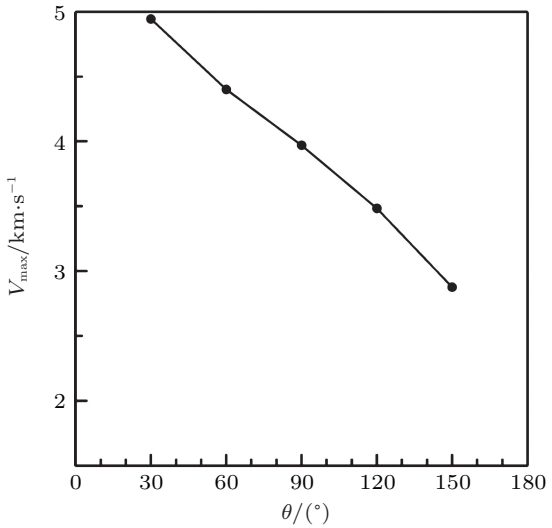


Fig. 9. Maximum ejecta velocity versus grooved angle.

5. Conclusion

We have discussed the dynamic failure and ejection characteristics of a periodic grooved Sn surface under unsupported shock loading by a smoothed particle hydrodynamics method. An "Eiffel Tower" spatial structure is observed, which includes high-speed jet tip, high-density jet slug, longitudinal tensile sparse zone, and complex broken zone between grooves. It is quite different from the spike–bubble spatial structure under supported shocks and has been validated by detonation loading experiments. In contrast with the supported shock cases with similar peak pressure, the high-speed ejecta decreases under unsupported shocks and the truncated location of ejection moves towards the interior of Sn sample obviously, while the total mass of ejecta increases due to the vast existence of low-speed broken materials. The main mechanisms for these differences are the interaction of complex wave system and the deduction of shock pressure of unsupported shocks. Finally, we have studied the influence of interface defect angle on ejecta under unsupported shocks and found that the shock profile determines mainly the total ejection amount, while the variations of groove angle will significantly change the spatial distribution characteristics of middle- and high-speed ejecta. The maximum ejecta velocity shows a linear reduction with the increase of groove angle.

References

[1] Zellner M B, Grover M, Hammerberg J E, Hixson R S, Iverson A J, Macrum G S, Morley K B, Obst A W, Olson R T, Payton J R, Rigg P A, Routley N, Stevens G D, Turley W D, Veeser L and Buttler W T 2007 *J. Appl. Phys.* **102** 013522

[2] de Rességuirer T, Lescoute E, Sollier A, Prudhomme G and Mercier P 2014 *J. Appl. Phys.* **115** 043525

[3] Buttler W T, Oro D M, Preston D L, Mikaelian K O, Cherne F J, Hixson R S, Mariam F G, Morris C, Stone J B, Terrones G and Tupa D 2012 *J. Fluid Mech.* **703** 60
[4] Dimonte G, Terrones G, Cherne F J,Germann T C, Dupont V, Kadau K, Buttler W T, Oro D M, Morris C and Preston D L 2011 *Phys. Rev. Lett.* **107** 264502
[5] Orth C D 2016 *Phys. Plasmas* **23** 022706
[6] Zellner M B, Mcneil W V, Hammerberg J E, Hixson R S, Obst A W, Olson R T, Payton J R, Rigg P A, Routley N, Stevens G D, Turley W D, Veeser L and Buttler W T 2008 *J. Appl. Phys.* **103** 123502
[7] de Rességuirer T, Roland C, Prudhomme G, Lescoute E, Loison D and Mercier P 2016 *J. Appl. Phys.* **119** 185108
[8] Chen Y T, Hong R K, Chen H Y and Ren G W 2016 *Acta Phys. Sin.* **65** 026201 (in Chinese)
[9] Chen J, Jing F Q, Zhang J L and Chen D Q 2002 *Acta Phys. Sin.* **51** 2386 (in Chinese)
[10] Shao J L, Wang P, He A M, Duan S Q and Qin C S 2013 *J. Appl. Phys.* **113** 153501
[11] Shao J L, Wang P, He A M and Qin C S 2012 *Acta Phys. Sin.* **61** 184701 (in Chinese)
[12] Wang P, Shao J L and Qin C S 2009 *Acta Phys. Sin.* **58** 1064 (in Chinese)
[13] Wang P, Shao J L and Qin C S 2012 *Acta Phys. Sin.* **61** 234701 (in Chinese)
[14] Liu G R and Liu M B 2003 *Smoothed Particle Hydrodynamics: A Meshfree Particle Method* (London: World Scientific) pp.311–317
[15] Libersky L D, Randles P W, Carney T C and Dickinson D L 1997 *Int. J. Impact Engng.* **20** 525
[16] Liu M B, Liu G R, Zong Z and Lam K Y 2003 *Comput. Fluids* **32** 305
[17] Buttler W T, Oro D M, Dimonte G, Morris C, Teerones G, Bainbridge J R, Hogan G E, Hollander B, Holtkamp D, Kwiatkowski K, Marr-Lyon M, Mariam F, Merrill F E, Nedrow P, Saunders A, Schwartz C L, Stone B, Tupa D and Vogan-Mcneil W S 2009 *Proceedings NEDPC LLNL Livermore United States* 26–30 October, 2009 836